The 9th European Congress on Computational Methods in Applied Sciences and Engineering
ECCOMAS Congress 2024
3–7 June 2024, Lisboa, Portugal

HAWT EFFICIENCY INCREASE VIA ACTIVE FLOW CONTROL IMPLEMENTATION

Ahmad Nabhani[1], Mohammad Saemian[1] and Josep M Bergada[1]

[1] Department of Fluid Mechanics, Universitat Politècnica de Catalunya (UPC), 08034 Barcelona, Spain
e-mail: [ahmad.nabhani, mohammad.saemian, josep.m.bergada] @upc.edu

Key words: CFD, Finite Volume Method, Aerodynamics, Horizontal Axis Wind Turbine, Boundary Layer, Active Flow Control, Synthetic Jets.

Abstract: The present manuscript introduces a novel methodology which can be applied to any Horizontal Axis Wind Turbine (HAWT) in order to improve the power generated under any operating condition. The method consists of analyzing via 2D-URANS a considerable number of sections cut along the wind turbine blade in order to obtain the location where the boundary layer separates, its associated vortex shedding frequency and the peak to peak amplitude of the dynamics forces. The second step consists of implementing optimized active Flow Control (AFC) parameters to each section where the boundary layer is separated, in order to reattach it for the considered wind turbine operating conditions. The energy assessment proves that a considerable increase of net energy is obtained in each section where the boundary layer reattachment is achieved.

1 Introduction

Flow control techniques can generally be categorized as passive and active. The performance of passive flow control techniques is optimal only at design conditions. On the other hand, Active Flow Control (AFC) implementation is capable of delaying the boundary layer separation for a wide range of operating conditions. Wind turbine blades must face a variety of flow conditions during operation, thus it is doubtful whether passive control strategies can have a positive effect under all operating conditions. Active Flow Control techniques (requiring power input) remove the drawback associated with passive control at off-design conditions [1, 2, 3]. This sort of control is associated with adding/subtracting momentum to/from particular locations. Synthetic Jet Actuators (SJA) [3, 4, 5, 6, 7] or direct-barrier-discharge plasma actuators (DBD-PA)[8, 9, 10], are two of the main devices used in AFC implementations.

Among the different AFC techniques, synthetic jet actuators have the advantage of generating pulsating flow which combines suction and blowing phases, and they are capable of generating large momentum coefficients. Due to the fact that SJA's have achieved good results in the field of aeronautics, it is logical to think that their application can be expanded to control flow separation on HAWT blades. The application of SJA on rotating blades of wind turbines is not observed until the last decade. The first researchers to illustrate experimentally the influence of SJA on the aerodynamic performance of HAWTs were Stalnov et al. [11] and Maldonado et al. [12, 13].

Stalnov et al. [11] investigated experimentally and using hot wire sensors, the effectiveness of SJA on a modified IAI pr8-SE profile at Reynolds numbers between $2 \times 10^5 \leq Re \leq 8 \times 10^5$. An overall efficiency increase of about $5-15\%$ was observed. Maldonado et al. [12, 13], applied SJA to an S809 airfoil in order to control the unsteady loading for a non-rotating and fixed-pitch wind turbine blade. Reynolds numbers ranging between 7.1×10^4, and 2.38×10^5 were considered, the momentum coefficients employed were between $C_\mu = 1.34 \times 10^{-3}$ and $C_\mu = 5.97 \times 10^{-3}$. 14 SJA, distributed in three locations, near the root, around the middle, and at the blade tip were used. The highest influence on flow reattachment and vibration reduction was obtained when placing the SJA near the blade tip. In their second research, the airfoil considered was the NACA 4415, the number of SJA as well as their location was the same as in their previous research. The Reynolds number range was also the same but the momentum coefficients employed ranged between 9.72×10^{-4} and 1.05×10^{-2}. They noticed the structural vibrations were considerably reduced thanks to the use of SJA.

To investigate the effect of the SJA on the boundary layer separation delay and its associated downstream structures, WT studies using stereo Particle Image Velocimetry (PIV) and employing the S817 airfoil were done at $Re = 3.75 \times 10^5$ by Rice et al. [14]. The SJA were placed at $x/C = 0.35$, being the momentum coefficient $C\mu = 0.012$. A significant reduction in the hysteresis of the lift and pitching moment coefficient of 41% and 85% was respectively observed. Maldonado and Gupta [15], experimentally evaluated at $Re = 1 \times 10^6$ the performance of a real 3-rotor blade using the S809 airfoil. They placed 20 SJA actuators along the blade radius and employed laser Doppler Anomemtry (LDA) to analyze the flow performance at the SJA's exit. For an angular velocity of 500rpm and a pitch angle of 3°, the actuation of 20 SJA per blade decreased the power input to drive the rotor by 10.6%, the rotor efficiency increased by 28%.

The S809 profile employed in a small HAWT and considering suction was studied by [16, 17]. In both studies, simulations were performed using the $k-\omega$ SST turbulence model. In the former research a suction groove was located at $0.15C$ versus the leading edge. Thanks to the AFC implementation, the pressure difference between the suction and the pressure surfaces was increased, increasing as well the stability of the flow field. Improvements were particularly relevant at low radius sections, where large boundary layer separation exists. The power of the HAWT increased with the wind speed, obtaining an increase versus the base case of 225.56% for a wind speed of $20m/s$. The effectiveness of using a single suction slot or two suction slots combined with a blowing one was analyzed in [17]. Slots were located at $0.1C$ and $0.5C$ for the dual case, just the former one was used for the single case. Two momentum coefficients were considered and they observed that when using the larger momentum coefficient and the dual suction configuration, the net power output had a maximum increase. One of the most comprehensive numerical studies to investigate the performance of SJA on the SD7003 airfoil at Reynolds number $Re \approx 6 \times 10^4$ was done by Tousi et al. [3, 4]. They optimized at four angles of attack (AoA) 4°, 6°, 8°, and 14° and using an in-house Genetic Algorithms optimizer, the five AFC parameters, jet position, jet with, momentum coefficient, frequency, and jet injection angle. They observed that aerodynamic efficiency could be increased by 251% at $AoA = 14°$ while a 39% increase was obtained at $AoA = 8°$. The same optimizer and optimization process is employed here to obtain the optimum AFC parameters for a given DTU-10MW-RWT airfoil.

2 Numerical method

In this research, we used the Unsteady Reynolds-Averaged Navier-Stokes (URANS) approach to properly detect the boundary layer dynamics. The finite volume CFD open-source package OpenFOAM was chosen to run all the simulations. A second order discretization method was used for all parameters. To connect pressure and velocity equations, the Pressure-Implicit with Splitting of Operators (PISO) scheme [18, 19] was employed.

In the context of incompressible flow, the only variables associated with the NS equations are the pressure and the three velocity components. Once each variable is substituted by its ensemble-averaged and its fluctuation terms, and after using the Boussinesq approximation, the Navier-Stokes equations can be expressed as:

$$\nabla \cdot \overline{\mathbf{u}} = 0 \tag{1}$$

$$\rho \frac{\partial \overline{\mathbf{u}}}{\partial t} + \rho \overline{\mathbf{u}} \cdot \nabla \overline{\mathbf{u}} = -\nabla \overline{p} + (\mu + \mu_t) \nabla^2 \overline{\mathbf{u}} \tag{2}$$

$\overline{\mathbf{u}}$ and $\overline{p}$ respectively represent the ensemble-averaged velocity vector and pressure, μ characterizes the kinematic viscosity and μ_t defines the turbulence viscosity. We decided to employ the $k-\omega$ SST turbulence model [20, 21]. This model incorporates the $k-\omega$ formulation in proximity to the wall, the $k-\epsilon$ model in regions far from the object, and a blending function bridging these two approaches. The turbulence viscosity μ_t can be defined as:

$$\mu_t = \frac{\rho k}{\omega} \quad \longrightarrow \quad \begin{cases} \rho : \text{density} \\ k : \text{turbulent kinetic energy} \\ \omega : \text{turbulent kinetic energy specific dissipation rate} \end{cases}$$

The model employs two transport equations to solve the k and ω variables. The governing equations for each parameter takes the form:

$$\frac{\partial k}{\partial t} + u_j \frac{\partial k}{\partial x_j} = P_k - \beta^* k\omega + \frac{\partial}{\partial x_j}\left[(\nu + \sigma_k \nu_T) \frac{\partial k}{\partial x_j} \right] \tag{3}$$

$$\frac{\partial \omega}{\partial t} + u_j \frac{\partial \omega}{\partial x_j} = \alpha S - \beta \omega^2 + \frac{\partial}{\partial x_j}\left[(\nu + \sigma_\omega \nu_T) \frac{\partial \omega}{\partial x_j} \right] + 2\,(1 - F_1)\,\sigma_{\omega 2} \frac{1}{\omega} \frac{\partial k}{\partial x_i} \frac{\partial \omega}{\partial x_i} \tag{4}$$

Two blending functions F_1 and F_2, are considered as a function of the distance from the cell to the wall. $F_1 = 0$ far from the wall, and $F_1 = 1$ near the wall, F_1 varies between 0 and 1 in the transition region. F_2 is a function of the perpendicular distance from the wall (d), and takes the form:

$$F_2 = \tanh\left(\arg_2^2\right) \tag{5}$$

$$\arg_2^2 = \max\left(\frac{2k}{\beta^* \omega d}; \frac{500\nu}{\omega d^2} \right) \tag{6}$$

In the present case, the following values were used: $\alpha_1 = 0.556$, $\alpha_2 = 0.44$, $\beta^* = 0.09$, $\beta_1 = 0.075$, $\beta_2 = 0.0828$, $\sigma_{k1} = 0.85$, $\sigma_{k2} = 1$, $\sigma_{\omega 1} = 0.5$, $\sigma_{\omega 2} = 0.856$. Further information of the $k-\omega\ SST$ turbulence model is to be found in [20].

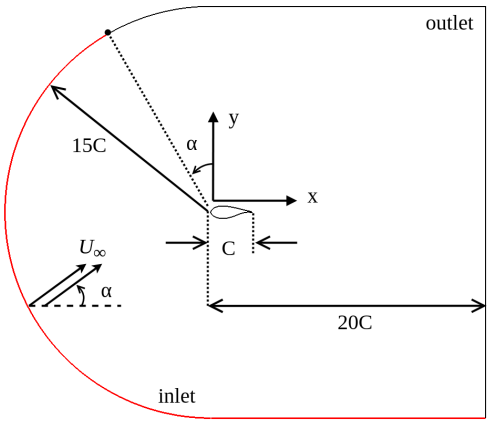

(a)

Figure 1: 2D Computational domain employed in the present study.

The computational domain used for all CFD simulations is the same as in [3] (see Figure 1). The origin of the coordinate system was placed at the corresponding airfoil leading edge. The computational domain upstream and downstream boundaries were set to 15 and 19 times the chord length (C), respectively. Each airfoil section was placed horizontally in the computational domain, the Angle of Attack (AoA) was set to zero degrees. To be able to consider the required AoA for each airfoil, the components of the relative velocity $(u, v) = (U_{\text{rel}} \cos\alpha, U_{\text{rel}} \sin\alpha)$ were set at the domain inlet. U_{rel} being the relative speed, calculated using the blade element momentum theory [22, 23, 24, 25, 26]. The boundary conditions for the velocity were Dirichlet at the computational domain inlet and at the synthetic jet groove, for the cases where AFC was considered. Velocity was set as null at the airfoil surface and Newmann boundary conditions were set at the computational domain outlet.

The time-dependent, top hat, velocity profile employed at the synthetic jet actuator was defined as: $u_j = U_j \sin(2\pi F t)$, U_j being the maximum jet velocity, F characterizes the jet frequency, and t is the dimensional time. Neumann boundary conditions for pressure were used at the computational domain inlet, synthetic jet, and airfoil walls, and Dirichlet boundary conditions for pressure were used at the computational domain outlet. After performing the mesh independence study we end up with a mesh of about 300K cells and a maximum $Y+$ of about 0.7.

3 Baseline results

Figure 2 represents the five airfoils evaluated in the present study and for a wind speed of $10m/s$, which covers from a very small $z/R = 0.1$ to a very large $z/R = 0.9$ non-dimensional blade radius. After performing the corresponding simulations, the resulting time-averaged pressure and friction coefficients are introduced in Figure 3. It can be observed that, for small blade radius the boundary layer is separated and the separation points move towards the trailing edge as the non dimensional radius z/R increases. Note that at $z/R = 0.5$ there is a minor separation of the flow at the airfoil trailing edge. It is also interesting to observe that when the bound-

ary layer is separated the pressure on the upper airfoil surface is particularly high, therefore drastically reducing the lift generated by the airfoil.

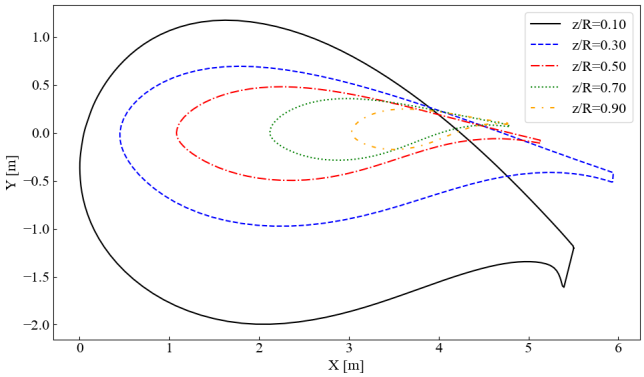

Figure 2: Airfoil sections distributed along the balde.

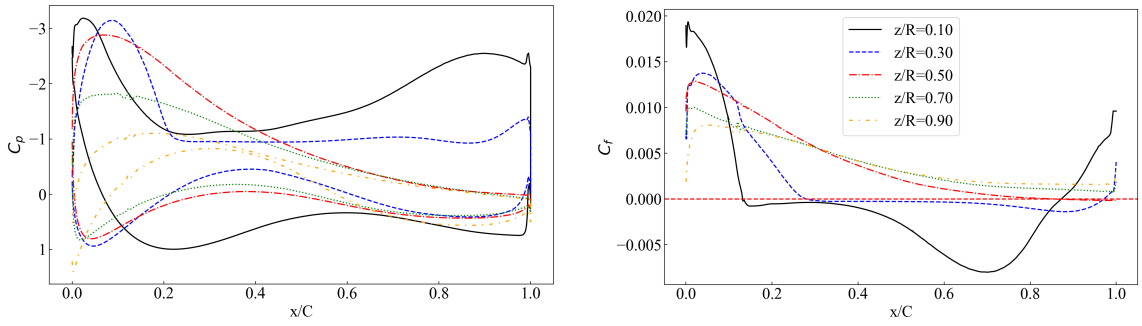

(a) C_p (b) C_f

Figure 3: Pressure and skin friction coefficients for the baseline cases studied.

A perhaps more intuitive way to visualize the flow performance on the top of each airfoil, consists of visualizing the time-averaged streamlines, and for the five airfoils considered this is presented in Figure 4. Now, the boundary layer separation and the time-averaged vortical structures forming onto the airfoil upper surface are clearly observed at $z/R = 0.1$ and $z/R = 0.3$. It is also seen a secondary vortical structure forming at these two airfoils trailing edge, this secondary vortical structure, which turns anticlockwise, forms from the interaction of the flow below the airfoil and the corresponding one above it. In fact, this secondary vortical structure can already be estimated from the friction coefficient plot in Figure 3, then the C_f becomes positive at the airfoil trailing edge. The slight flow separation at $z/R = 0.5$ is now more clearly seen and clearly at higher radius, the boundary layer is fully attached.

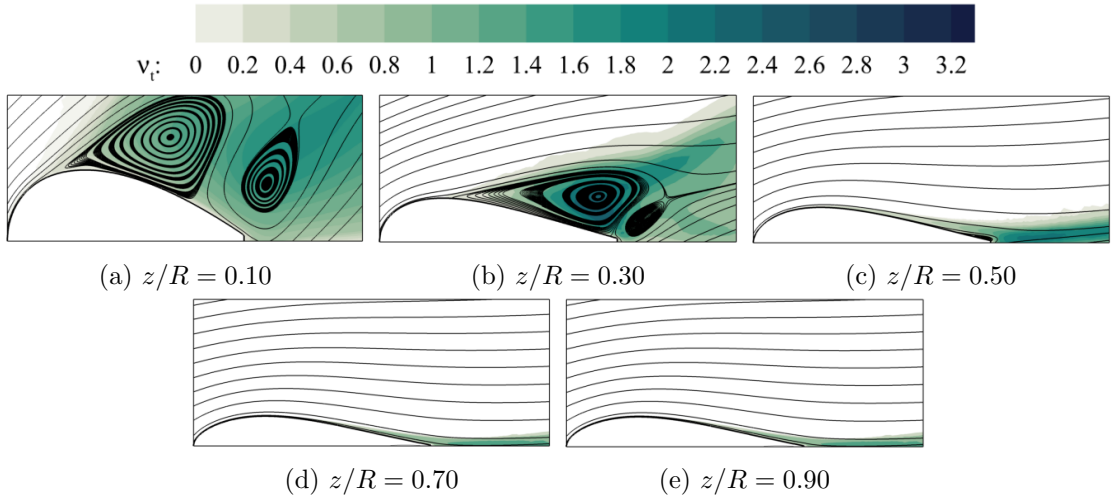

(a) $z/R = 0.10$ (b) $z/R = 0.30$ (c) $z/R = 0.50$

(d) $z/R = 0.70$ (e) $z/R = 0.90$

Figure 4: Averaged velocity streamlines.

4 AFC implementation results

Once the Baseline cases are studied and the boundary layer separation point as well as the associated vortex shedding frequency are obtained for each airfoil, the AFC implementation based on SJA's can be studied. At this point we focused on optimizing the five associated AFC parameters for the $z/R = 0.3$ case. The in-house Genetic Algorithm's (GA) optimizer used and the process followed to optimize the five AFC parameters is described in [3, 4]. In here, just the outcome of the optimization for the maximum lift and maximum efficiency cases is presented in Table 1. From where it is seen that injection angles of 5°, non-dimensional groove widths and frequencies of $h/C = 0.005$ and $F^+ \approx 5.5$, appear to be optimal to maximize the lift as well as the efficiency of the airfoil. In fact, small variations of the jet position x_j/C and the momentum coefficient C_μ are sufficient to maximize whether the lift or the efficiency. Is is as well relevant to see that lift coefficients and efficiencies increase, versus the baseline case, of over 80% and 428% can be obtained when reattaching the boundary layer in this particular section. In fact, the boundary layer reattachment for both optimized cases and when compared with the baseline one is presented in Figure 5. For both optimum cases the boundary layer is almost fully reattached along the entire airfoil upper surface, in fact a slightly better reattachment is observed for the maximum lift case, and this is also seen in Table 1, then the lift coefficient increase is of over 90% under this conditions. Maximum efficiency appears to be related to a small boundary layer separation at the airfoil trailing edge.

Table 1: Optimum AFC parameters obtained for the maximum lift and maximum efficiency cases and for the airfoil considered $z/R = 0.30$

z/R	Cases	F^+	C_μ	$\theta°$	x_j/C	h/C	C_L	C_L%	η	η%
0.30	Max lift	5.41	0.0098	5	0.32	0.005	2.99	90.44	30.73	428.00
	Max efficiency	5.64	0.0093	5	0.29	0.005	2.84	80.89	32.47	457.90
	Baseline	-	-	-	-	-	1.57	-	5.82	-

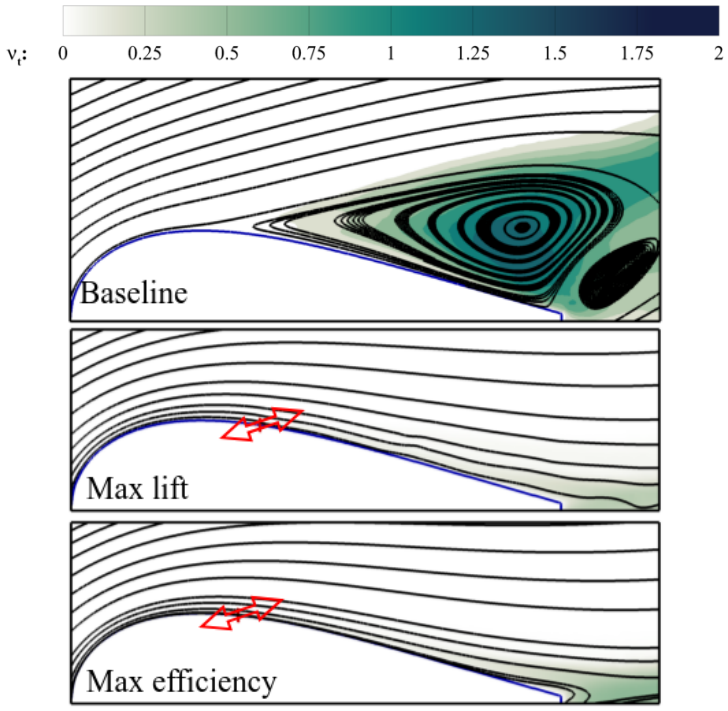

(a) $z/R = 0.30$

Figure 5: Averaged velocity streamlines before and after optimization for the $z/R = 0.30$ airfoil.

5 Energy assessment

To evaluate how effective is the AFC implementation, an energy evaluation is needed and consists in comparing the power needed for the SJ with the power gained by the airfoil. The power needed to activate the synthetic jet is defined as [3, 27]:

$$W_j = \frac{1}{2}\rho_j A_j \sin\theta_{\text{jet}} \overline{u_j^3} \tag{7}$$

Where ρ_j characterizes the density of the exiting fluid, A_j defines the cross-sectional flow area of the synthetic jets and $\overline{u_j^3}$ represents the jet time-dependent velocity profile defined as [27, 28]:

$$\overline{u_j^3} = \frac{4}{3\pi} U_j^3 \tag{8}$$

The incremental torque represents the difference between the torque generated by the actuated airfoil and the baseline one. It is initially essential to determine the resultant aerodynamic force (F_{Tr}) for both cases, which is obtained by decomposing the lift and drag forces in the plane of rotation using the inflow angle (φ). It is important to note that the provided aerodynamic coefficients represent the corresponding time-averaged values.

$$F_{Tr\,AFC} = \frac{1}{2}\rho_\infty u_{rel}^2 c \left(c_{l_{AFC}} \sin\varphi - c_{d_{AFC}} \cos\varphi\right) \tag{9}$$

$$F_{Tr\,BSC} = \frac{1}{2}\rho_\infty u_{rel}^2 c\left(c_{l_{BCS}}\sin\varphi - c_{d_{BCS}}\cos\varphi\right) \tag{10}$$

By considering the forces generated in both the actuated and baseline cases, the increase in the power generated by the airfoil can be determined.

$$\Delta W = r\cdot\Omega\cdot\left(F_{Tr\,AFC} - F_{Tr\,BCS}\right) \tag{11}$$

The net power balance (W_G) is obtained when considering the incremental power (ΔW) obtained from each of the airfoils optimized and the power needed to delay the boundary layer separation (W_j):

$$W_G = \Delta W - W_j \tag{12}$$

Table Table 2 summarizes the net power gain W_G obtained by the airfoil considered and when the maximum lift and maximum efficiency cases are considered. In both cases the net power gain is very similar and represents about 20 times the power needed for the AFC implementation. Clearly, the extension of this study to the rest of the airfoils where the boundary layer is separated, will highlight the overall power increase the wind turbine is capable of generating.

Table 2: Net power ratio obtained for the optimum cases

z/R	Case	U_j/U_{rel}	$W_J[kW]$	ΔW [kW]	W_G [kW]
z/R=0.30	Max C_l	4.5	1.85	37.91	36.07
	Max η	4.4	1.77	36.06	34.3

6 Conclusions

In this paper, we have analyzed via URANS the flow at different sections of a HAWT and for a wind velocity of $10m/s$. We have detected the airfoils where the boundary layer is separated and we have optimized for one of the airfoils all five AFC parameters which maximize the lift and efficiency of the airfoil. From the simulation of the chosen airfoil with the optimized AFC parameters we managed to reattach the boundary layer, incrementing the lift coefficient versus the baseline case of over 80% and the efficiency of over 428%. Which clearly shows that the extension of the study to the rest of the airfoils is needed and will very likely bring a cosiderable increase of the power generated by the turbine.

REFERENCES

[1] G. Jones, M. Santer, and G. Papadakis, "Control of low reynolds number flow around an airfoil using periodic surface morphing: A numerical study," *Journal of Fluids and Structures*, vol. 76, pp. 95–115, 2018.

[2] A. Rezaeiha, H. Montazeri, and B. Blocken, "Active flow control for power enhancement of vertical axis wind turbines: Leading-edge slot suction," *Energy*, vol. 189, p. 116131, 2019.

[3] N. Tousi, M. Coma, J. Bergadà, J. Pons-Prats, F. Mellibovsky, and G. Bugeda, "Active flow control optimization on sd7003 airfoil at pre and post-stall angles of attack using synthetic jets," *Applied Mathematical Modelling*, vol. 98, pp. 435–464, 2021.

[4] N. Tousi, J. Bergadà, and F. Mellibovsky, "Large eddy simulation of optimal synthetic jet actuation on a sd7003 airfoil in post-stall conditions," *Aerospace Science and Technology*, p. 107679, 2022.

[5] M. Amitay, D. R. Smith, V. Kibens, D. E. Parekh, and A. Glezer, "Aerodynamic flow control over an unconventional airfoil using synthetic jet actuators," *AIAA journal*, vol. 39, no. 3, pp. 361–370, 2001.

[6] N. Buchmann, C. Atkinson, and J. Soria, "Influence of znmf jet flow control on the spatio-temporal flow structure over a naca-0015 airfoil," *Experiments in fluids*, vol. 54, pp. 1–14, 2013.

[7] W. Zhang and R. Samtaney, "A direct numerical simulation investigation of the synthetic jet frequency effects on separation control of low-re flow past an airfoil," *Physics of Fluids*, vol. 27, no. 5, 2015.

[8] J.-J. Wang, K.-S. Choi, L.-H. Feng, T. N. Jukes, and R. D. Whalley, "Recent developments in dbd plasma flow control," *Progress in Aerospace Sciences*, vol. 62, pp. 52–78, 2013.

[9] M. Sato, T. Nonomura, K. Okada, K. Asada, H. Aono, A. Yakeno, Y. Abe, and K. Fujii, "Mechanisms for laminar separated-flow control using dielectric-barrier-discharge plasma actuator at low reynolds number," *Physics of Fluids*, vol. 27, no. 11, 2015.

[10] M. G. De Giorgi, A. Ficarella, F. Marra, and E. Pescini, "Micro dbd plasma actuators for flow separation control on a low pressure turbine at high altitude flight operating conditions of aircraft engines," *Applied Thermal Engineering*, vol. 114, pp. 511–522, 2017.

[11] O. Stalnov, A. Kribus, and A. Seifert, "Evaluation of active flow control applied to wind turbine blade section," *Journal of Renewable and Sustainable Energy*, vol. 2, no. 6, 2010.

[12] V. Maldonado, M. Boucher, R. Ostman, and M. Amitay, "Active vibration control of a wind turbine blade using synthetic jets.," *International Journal of Flow Control*, vol. 1, no. 4, 2009.

[13] V. Maldonado, J. Farnsworth, W. Gressick, and M. Amitay, "Active control of flow separation and structural vibrations of wind turbine blades," *Wind Energy: An International Journal for Progress and Applications in Wind Power Conversion Technology*, vol. 13, no. 2-3, pp. 221–237, 2010.

[14] T. T. Rice, K. Taylor, and M. Amitay, "Wind tunnel quantification of dynamic stall on an s817 airfoil and its control using synthetic jet actuators," *Wind Energy*, vol. 22, no. 1, pp. 21–33, 2019.

[15] V. Maldonado and S. Gupta, "Increasing the power efficiency of rotors at transitional reynolds numbers with synthetic jet actuators," *Experimental Thermal and Fluid Science*, vol. 105, pp. 356–366, 2019.

[16] P. Wang, Q. Liu, C. Li, W. Miao, M. Yue, and Z. Xu, "Investigation of the aerodynamic characteristics of horizontal axis wind turbine using an active flow control method via boundary layer suction," *Renewable Energy*, vol. 198, pp. 1032–1048, 2022.

[17] Y. Sun, Y. Qian, Y. Gao, T. Wang, and L. Wang, "Stall control on the wind turbine airfoil via the single and dual-channel of combining bowing and suction technique," *Energy*, vol. 290, p. 130224, 2024.

[18] R. I. Issa, A. Gosman, and A. Watkins, "The computation of compressible and incompressible recirculating flows by a non-iterative implicit scheme," *Journal of Computational Physics*, vol. 62, no. 1, pp. 66–82, 1986.

[19] H. K. Versteeg and W. Malalasekera, *An introduction to computational fluid dynamics: the finite volume method*. Pearson education, 2007.

[20] F. Menter and C. Rumsey, "Assessment of two-equation turbulence models for transonic flows," in *Fluid Dynamics Conference*, p. 2343, 1994.

[21] F. R. Menter, M. Kuntz, R. Langtry, *et al.*, "Ten years of industrial experience with the sst turbulence model," *Turbulence, heat and mass transfer*, vol. 4, no. 1, pp. 625–632, 2003.

[22] W. J. M. Rankine, "On the mechanical principles of the action of propellers," *Transactions of the Institution of Naval Architects*, vol. 6, 1865.

[23] R. E. Froude, "On the part played in propulsion by differences of fluid pressure," *Trans. Inst. Naval Architects*, vol. 30, p. 390, 1889.

[24] R. E. Wilson and P. B. Lissaman, "Applied aerodynamics of wind power machines," *Renewable Energy*, pp. Vol3_71–Vol3_120, 2018.

[25] M. Hansen, *Aerodynamics of wind turbines*. Routledge, 2015.

[26] T. Burton, N. Jenkins, D. Sharpe, and E. Bossanyi, *Wind energy handbook*. John Wiley & Sons, 2011.

[27] M. De Giorgi, C. De Luca, A. Ficarella, and F. Marra, "Comparison between synthetic jets and continuous jets for active flow control: application on a naca 0015 and a compressor stator cascade," *Aerospace Science and Technology*, vol. 43, pp. 256–280, 2015.

[28] M. G. De Giorgi, S. Traficante, C. De Luca, D. Bello, and A. Ficarella, "Active flow control techniques on a stator compressor cascade: a comparison between synthetic jet and plasma actuators," in *Turbo Expo: Power for Land, Sea, and Air*, vol. 44748, pp. 439–450, American Society of Mechanical Engineers, 2012.